Supplementary Information

A New Mechanism of Acid Rain Generation from HOSO at the Air-Water Interface

Manuel F. Ruiz-López,[a],* Marilia T. C. Martins-Costa,[a] Josep M. Anglada[b] and Joseph S. Francisco[c]

a] Laboratoire de Physique et Chimie Théoriques, UMR CNRS 7019, University of Lorraine, CNRS, BP 70239, 54506 Vandoeuvre-lès-Nancy, France
[b] Departament de Química Biològica (IQAC), CSIC, c/ Jordi Girona 18, E-08034 Barcelona, Spain
[b] Department of Earth and Environmental Science and Department of Chemistry, University of Pennsylvania, Philadelphia, PA, USA 19104-6316

Summary

1. QM/MM simulations

Molecular Dynamics (MD) simulations were carried out using a combined molecular dynamics and quantum mechanics force-field described in previous work.[1] We used the hybrid QM/MM approach[2,3] developed in our group.[4-7] In this scheme, the solute is described quantum mechanically (QM), the solvent is described classically using molecular mechanics (MM), and we allow for QM/MM electrostatic embedding. We assume the Born-Oppenheimer approximation and nuclei movements are treated classically. Quantum effects have been sometimes incorporated in MD simulations involving proton transfers but they are not expected to significantly affect the results reported in this work. For instance, an estimation of the tunneling effect via Wigner approach leads to a factor of 1.3 for the kinetic constant in the ionization process in the cluster calculations below, which is a small effect.

The simulations were carried out in the NVT ensemble (T=298K, Nosé–Hoover thermostat[8,9]) using a box containing the solute and 499 water molecules. The box size is (in Å) 24.685 x 24.685 x 130. Periodic boundary conditions are used along the X and Y directions. The solute is described at the B3LYP level[10] using the 6-311+G(d) basis set.[11-13] Water molecules are described using the TIP3P model.[14] We use the Gaussian 09 program[15] for the QM calculations, Tinker 4.2[16] for the MD simulations and the interface developed by the group of Nancy.[17] The time step is 0.25 fs. After equilibration, the simulation is carried out for several tenths of picosenconds. Two simulations were carried out:

Simulation 1. The solute (QM system) is HOSO. Simulation time is 100 ps

Simulation 2. The solute (QM system) is the complex HOSO···H_2O. After slightly less than 30 ps the system is ionized. Since only one water molecule is the QM part, the simulation is stopped afterwards, as simulating proton diffusion processes is not realistic in this model.

2. Structure of HOSO at the air-water interface.

The minimum energy structure of HOSO in the gas phase displays a non-planar *syn* configuration but the energy surface between planar *cis* and *syn* structures is extremely flat. Previous studies showed that results for the dihedral angle strongly depend on method: δ=24.2° at ROH-CCSD(T) level [18,19] vs δ=54.7° at CASPT2 level,[20] for instance. Recommended *cis* and *trans* rotational barriers[19] are 5 cm^{-1} and 2.3 $kcal \cdot mol^{-1}$, respectively. The reported dipole moment is 1.17 D.[21]

The energy surface associated to the dihedral angle δ calculated in this work is shown in Figure S1. Values at the interface have been obtained from Simulation 1. As shown, solvation produces large modifications of the energy surface. It preferentially stabilizes larger δ configurations because they are more polar. The final result is that the equilibrium dihedral angle of HOSO increases by more than 20° at the interface with respect to gas phase. The cis barrier raises and the trans barrier lowers but both are similar and small (below 1 kcal·mol-1) and therefore rotation around the HO-SO bond is almost free. The results of simulation 1 also show that HOSO has significant air-water interface affinity, as revealed by the free energy profile displayed in Figure S2.

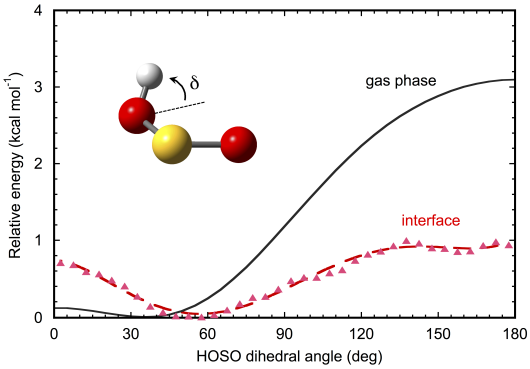

Figure S1. Energy curves with respect to the dihedral angle in HOSO. Gas-phase values correspond to a relaxed potential energy scan at B3LYP/6-3111+G(d) level. Interface values correspond to free energy variation from QM/MM simulation 1 at the same QM level. Energy minima are obtained for dihedral angle equal 35° (gas phase) and 57.5° (air-water interface).

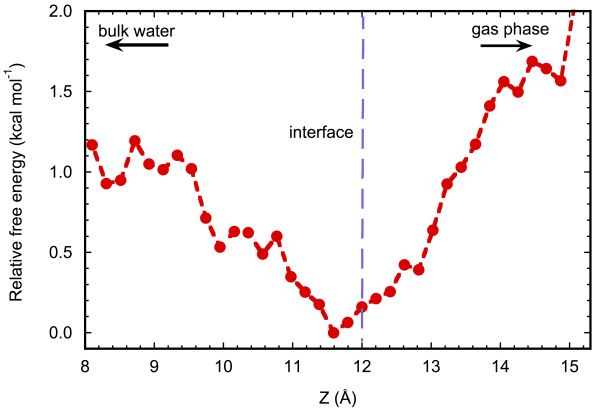

Figure S2. Free energy profile for HOSO accommodation at the air-water interface at 298K. Z is the distance between the HOSO center of mass and the center of mass of the simulation box. The formal interface is at Z=12 Å. The free energy profile is obtained from simulation 1 and the probability distribution of Z.

3. Cluster calculations

B3LYP/6-311+G(d) calculations have been carried out to study HOSO dissociation on a $(H_2O)_{21}$ cluster similar to those carried out for HO_2 in a previous work.[22] We use the Gaussian 09 program.[15] After locating the transition state for the process, intrinsic reaction coordinate calculations[23] have been carried out to analyze the elementary steps of the process along the reaction coordinate. The results for the potential energy surface are shown in Figure S3. The Figure shows that the ionization process starts by a transfer from HOSO to the nearest water molecule (structure a in the Figure) and is followed by 3 water-to-water proton transfers (b-d). The formal transition state (characterized by a vibrational analysis) corresponds to structure b and lies 8.8 kcal mol^{-1} above the reactant complex. The product lies 1.2 kcal mol^{-1} above the reactant complex. These values correspond to potential energies and do not take into account neither zero-point energies nor thermal corrections.

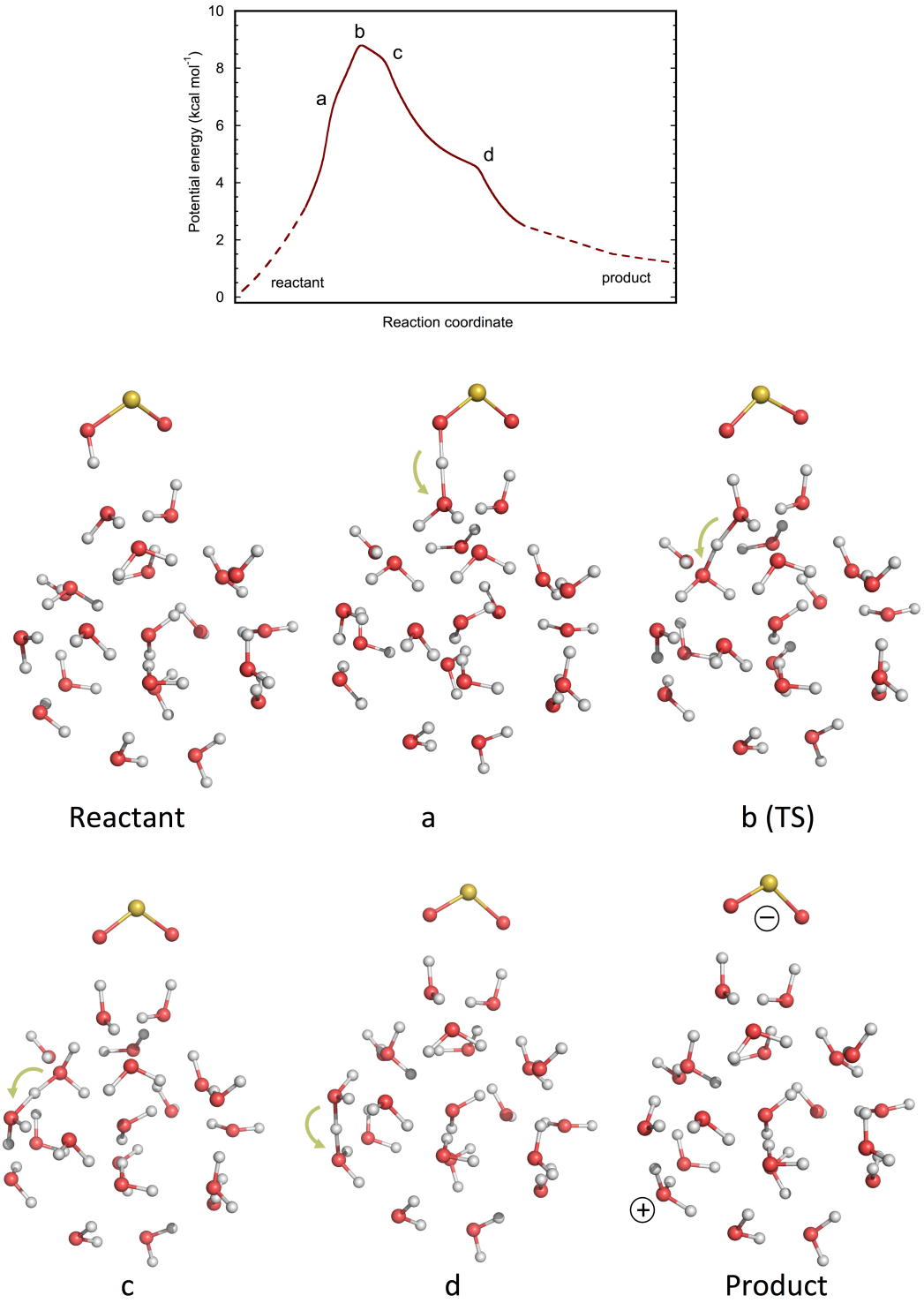

Figure S3. Energy profile along the reaction coordinate for HOSO ionization in the $(H_2O)_{21}$ water cluster calculated by the IRC method at the B3LYP/6-311+G(d) level. The dashed lines have been added to join the fully optimized reactant and product form the last points of the IRC calculations. Structures along the reaction path correspond to elementary proton transfer processes.

4. Calculation of HOSO and HONO acidities

Gas phase HONO and HOSO acidities. The geometry of HOXO and XO_2^- species (X=N,S) were optimized at the MP2/ aug-cc-pVTZ level of theory, which was also used to calculate vibrational frequencies, zero-point energy and thermal contribution to free energy. The electronic energy was recalculated at the CCSD(T)/aug-cc-pVTZ level of theory using the MP2 geometries. This theoretical level is abbreviated CCSD(T)//MP2. The total energies are summarized in Table S1. The gas phase free energy of the proton is $G(H^+)$ = -6.28 kcal/mol. All quantities are calculated at 1 atm, 298K using the Gaussian 09 program.[15]

Aqueous phase acidities, pK_a. The ab initio level was similar to that used in gas phase. The calculations in solution are done using the implicit PCM model[24] as described in detail in previous works (see for instance reference[25]). The free energy of solvation is approximated by the electrostatic and non-electrostatic terms, and includes geometry relaxation. Zero-point and thermal contributions to the solvation free energy are neglected (in other words, we assume the gas-phase values for the free energy computations in solution). The pK_a is defined in the following way:

$$HOXO \rightarrow H^+ + OXO^- \quad (X=N, S) \tag{13}$$

$$\Delta G_{water} = \Delta G_{gas}\,(1\ atm) + \delta\Delta G_{solv}(1\ atm \rightarrow 1M) \tag{14}$$

where $\Delta G_{solv}(1\ atm \rightarrow 1M)$ is the solvation energy from 1 atm in gas phase to 1 M reference state in solution. The last term accounts for the difference in solvation energy between the products ($H^+ + OXO^-$) and the reactant (HOXO) in the dissociation process. The solvation energy for the proton is $\Delta G_{solv}(H^+)$ = -264.0 kcal mol^{-1} for the 1 atm → 1 M process.[25] Finally:

$$pK_a = \frac{\Delta G_{water}}{2.303\ RT} \tag{15}$$

Absolute pK_a are normally affected by significant errors. In the present case, the calculated absolute pK_a of HONO is almost one unit larger than the experimental value (4.1 vs 3.16). Main errors come from the computational model, the theoretical level, and the free energy of the solvated proton. Due to error compensation, however, relative pK_a calculations are much more accurate (in addition, they are independent of proton energy). In this work, the pK_a of HOSO has been calculated relative to the pK_a of HONO, i. e. we consider the process:

$$HOSO + ONO^- \rightarrow OSO^- + HONO \tag{16}$$

The pK_a is obtained using the experimental pK_a of HONO plus the calculated ΔpK_a.

Table S1. Gas-phase potential and free energies (in au) and energy differences (in kcal mol^{-1}) at MP2/aug-cc-pVTZ level and CCSD(T)/aug-cc-pVTZ levels of theory. For comparison, energies of HOSO and SO_2^- at the B3LYP/6-311+G(d) level used in the simulations are also included.

	E B3LYP	G B3LYP	E MP2	G MP2	E CCSD(T)//MP2	G CCSD(T)//MP2
HONO	-205.7639225	-205.767804	-205.4205368	-205.424633	-205.45144653	-205.45553589
NO_2^-	-205.2249931	-205.240187	-204.8743725	-204.889528	-204.89874268	-204.91389465
Δ	338.2	331.1	342.7	335.8	346.8	339.9
HOSO	-549.252624	-549.262819	-548.5298682	-548.539365	-548.5698392	-548.57933600
SO_2^-	-548.724960	-548.744623	-548.002081	-548.021432	-548.0349268	-548.05427780
Δ	331.1	325.2	331.2	325.0	335.7	329.5

5. Estimation of $[SO_2^-]$ and $[H^+]$ production rates

The relevant processes and kinetic constants for the photochemistry of SO_2 at the air water interface are gathered in **Table S2.** It is worth reminding that the lowest triplet state of SO_2 has a large lifetime, $\tau = (7.9 \pm 1.7)\ 10^{-4}$ s.[26]

The upper limit for $[SO_2^-]$ and $[H^+]$ formation rate is connected to the absorption rate in the troposphere. Using the calculated value for J_1,[1] this leads to 0.2×10^{10} molecule·cm^{-3}·s^{-1} (ppb $[SO_2]_g)^{-1}$, where the gas phase concentration $[SO_2]_g$ is related to the interface concentration by[1] $[SO_2]_{interface} = 2.2 \times 10^2\ [SO_2]_g$.

To obtain a more accurate estimation, the kinetic equations reported by Kroll et al[27] together with the kinetic constants in Table S2 can be used. However some approximations are necessary. We will assume that the rate of $[SO_2^-]$ and $[H^+]$ formation is approximately equal to the formation rate of the radical HOSO, ν_{HOSO}, since dissociation of this radical is fast and complete. Values for ν_{HOSO} were already reported for different gas phase concentrations of SO_2 in our previous work.[1] In that study, the rate of reaction (12) was taken from gas phase experiments.[27] However, we have recently shown that the reaction is significantly accelerated by the effect of solvation.[28] Actually, the activation free energy barrier for the process is very small (around 0.7 kcal·mol^{-1}) and accordingly, the rate of reaction (12) should be limited by diffusion. Typical rate constant values for near-diffusion-controlled reactions in water at room temperature are around 10^{-10} cm^3·molecule^{-1}·s^{-1}.[29] Using these data, one deduces a HOSO formation rate that is only one order of magnitude smaller than the upper limit obtained from the absorption rate, though the result is not very accurate because it strongly depends on the singlet quenching kinetic constants k_9 and k_{10}, ($\nu_{HOSO} \approx \frac{J_1 k_9}{k_{10}} [SO_2]_{interface}$) for which only approximate values are available. The production rate as a function of wavelength is plotted in Figure S4 (we assume the upper limit rate) and displays a maximum in the 310-315 nm region.

Table S2. Reactions and rate constants considered for the photochemical formation of HOSO at the air-water interface (values taken from Kroll et al[27] unless otherwise stated). At the air-water interface, [M]≈[H_2O]≈1.7 10^{22} molecule·cm^{-3}.

1) $SO_2 + h\nu \longrightarrow {}^1SO_2$	$J_1 = 4 \times 10^{-4}$ s^{-1} (reference[1])
2) $SO_2 + h\nu \longrightarrow {}^3SO_2$	$J_2 = 2.2 \times 10^{-6}$ s^{-1}
3) ${}^1SO_2 \longrightarrow SO_2 + h\nu$	$k_3 = 2.2 \times 10^4$ s^{-1}
4) ${}^3SO_2 \longrightarrow SO_2 + h\nu$	$k_4 = 1.1 \times 10^3$ s^{-1}
5) ${}^1SO_2 \longrightarrow {}^3SO_2$	$k_5 = 1.5 \times 10^3$ s^{-1}
6) ${}^1SO_2 + SO_2 \longrightarrow SO_2 + SO_2$	$k_6 = 2.9 \times 10^{-11}$ cm^3 · molecule^{-1} · s^{-1}
7) ${}^1SO_2 + SO_2 \longrightarrow {}^3SO_2 + SO_2$	$k_7 = 3.0 \times 10^{-12}$ cm^3 · molecule^{-1} · s^{-1}
8) ${}^3SO_2 + SO_2 \longrightarrow SO_2 + SO_2$	$k_8 = 5.8 \times 10^{-13}$ cm^3 · molecule^{-1} · s^{-1}
9) ${}^1SO_2 + M \longrightarrow {}^3SO_2 + M$	$k_9 \sim 1 \times 10^{-12}$ cm^3 · molecule^{-1} · s^{-1}
10) ${}^1SO_2 + M \longrightarrow SO_2 + M$	$k_{10} \sim 1 \times 10^{-11}$ cm^3 · molecule^{-1} · s^{-1}
11) ${}^3SO_2 + M \longrightarrow SO_2 + M$	$k_{11} = 1.1 \times 10^{-13}$ cm^3 · molecule^{-1} · s^{-1}
12) ${}^3SO_2 + H_2O \longrightarrow OH + HOSO$	$k_{12} \sim 10^{-10}$ cm^3 · molecule^{-1} · s^{-1} (diffusion control assumed)
13) ${}^1SO_2 + SO_2 \longrightarrow SO + SO_3$	$k_{13} = 4 \times 10^{-12}$ cm^3 · molecule^{-1} · s^{-1}
14) ${}^3SO_2 + SO_2 \longrightarrow SO + SO_3$	$k_{14} = 7 \times 10^{-14}$ cm^3 · molecule^{-1} · s^{-1}
15) $SO + SO_3 \longrightarrow 2SO_2$	$k_{15} = 1.0 \times 10^{-15}$ cm^3 · molecule^{-1} · s^{-1}

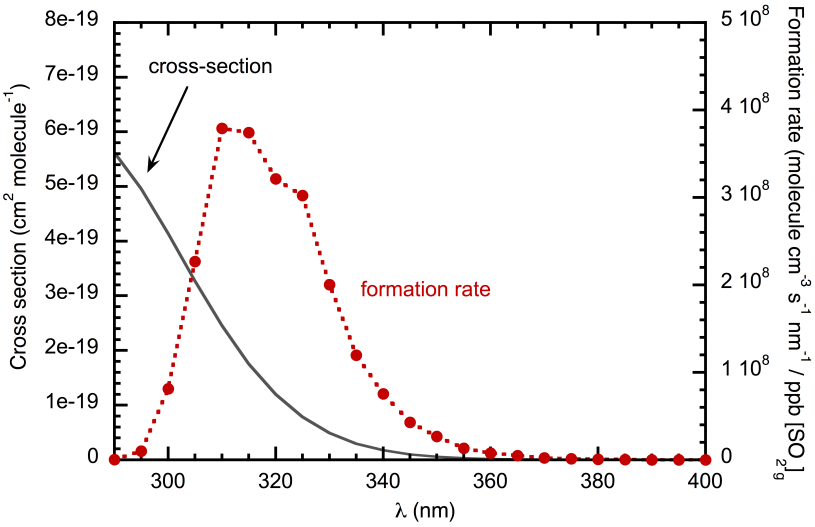

Figure S4. HOSO production rate at the air-water interface as a function of wavelength calculated using data for cross-section reported in our previous work[1], actinic flux from reference,[30] and assuming an upper limit rate, as explained in the text. The HOSO formation rate is then assumed to be also the formation rate of SO_2^- radical anion and H^+.

6. References

(1) Martins-Costa, M. T.; Anglada, J. M.; Francisco, J. S.; Ruiz-López, M. F. *J. Am. Chem. Soc.* **2018**, *140*, 12341-12344.
(2) Field, M. J.; Bash, P. A.; Karplus, M. *J. Comput. Chem.* **1990**, *11*, 700-733.
(3) Warshel, A.; Levitt, M. *J. Mol. Biol.* **1976**, *103*, 227-249.
(4) Tuñón, I.; Martins-Costa, M. T. C.; Millot, C.; Ruiz-Lopez, M. F. *Chem. Phys. Lett.* **1995**, *241*, 450-456.
(5) Tuñón, I.; Martins-Costa, M. T. C.; Millot, C.; Ruiz-López, M. F. *J. Mol. Mod.* **1995**, *1*, 196-201.
(6) Tuñón, I.; Martins-Costa, M. T. C.; Millot, C.; Ruiz-López, M. F. *J. Chem. Phys.* **1997**, *106*, 3633-3642.
(7) Tuñón, I.; Martins-Costa, M. T. C.; Millot, C.; Ruiz-López, M. F.; Rivail, J. L. *J. Comp. Chem.* **1996**, *17*, 19-29.
(8) Hoover, W. G. *Phys. Rev. A* **1985**, *31*, 1695-1697.
(9) Nosé, S. *J. Chem. Phys.* **1984**, *81*, 511-519.
(10) Becke, A. D. *J. Chem. Phys.* **1993**, *98*, 5648-5652.
(11) Hehre, W. J.; Ditchfield, R.; Pople, J. A. *J. Chem. Phys.* **1972**, *56*, 2257-2261.
(12) Hehre, W. J.; Stewart, R. F.; Pople, J. A. *J. Chem. Phys.* **1969**, *51*, 2657-2664.
(13) Krishnan, R.; Binkley, J. S.; Seeger, R.; Pople, J. A. *J. Chem. Phys.* **1980**, *72*, 650-654.
(14) Jorgensen, W. L.; Chandrashekar, J.; Madura, J. D.; Impey, W. R.; Klein, M. L. *J. Chem. Phys.* **1983**, *79*, 926-935.
(15) Frisch, M. J.; Trucks, G. W.; Schlegel, H. B.; Scuseria, G. E.; Robb, M. A.; Cheeseman, J. R.; Scalmani, G.; Barone, V.; Mennucci, B.; Petersson, G. A.; Nakatsuji, H.; Caricato, M.; Li, X.; Hratchian, H. P.; Izmaylov, A. F.; Bloino, J.; Zheng, G.; Sonnenberg, J. L.; Hada, M.; Ehara, M.; Toyota, K.; Fukuda, R.; Hasegawa, J.; Ishida, M.; Nakajima, T.; Honda, Y.; Kitao, O.; Nakai, H.; Vreven, T.; Montgomery Jr., J. A.; Peralta, J. E.; Ogliaro, F.; Bearpark, M. J.; Heyd, J.; Brothers, E. N.; Kudin, K. N.; Staroverov, V. N.; Kobayashi, R.; Normand, J.; Raghavachari, K.; Rendell, A. P.; Burant, J. C.; Iyengar, S. S.; Tomasi, J.; Cossi, M.; Rega, N.; Millam, N. J.; Klene, M.; Knox, J. E.; Cross, J. B.; Bakken, V.; Adamo, C.; Jaramillo, J.; Gomperts, R.; Stratmann, R. E.; Yazyev, O.; Austin, A. J.; Cammi, R.; Pomelli, C.; Ochterski, J. W.; Martin, R. L.; Morokuma, K.; Zakrzewski, V. G.; Voth, G. A.; Salvador, P.; Dannenberg, J. J.; Dapprich, S.; Daniels, A. D.; Farkas, Ö.; Foresman, J. B.; Ortiz, J. V.; Cioslowski, J.; Fox, D. J. In *Gaussian 09*; Gaussian, Inc.: Wallingford, CT, USA, 2009.
(16) Ponder, J. W.; 4.2 ed.; Washington University School of Medicine: Saint Louis, MO.: 2004.
(17) Martins-Costa, M. T. C.; Ruiz-López, M. F. *Chem. Phys.* **2007**, *332*, 341-347.
(18) Rodríguez-Linares, D.; Freitas, G. N.; Ballester, M. Y.; Nascimento, M. A. C.; Garrido, J. D. *J. Phys. Chem. A* **2015**, *119*, 8734-8743.
(19) Wheeler, S. E.; Schaefer, H. F. *J. Phys. Chem. A* **2009**, *113*, 6779-6788.

(20) Garrido, J. D.; Ballester, M. Y.; Orozco-Gonzalez, Y.; Canuto, S. *J. Phys. Chem. A* **2011**, *115*, 1453-1461.
(21) McCarthy, M. C.; Lattanzi, V.; Martinez Jr, O.; Gauss, J. r.; Thorwirth, S. *J. Phys. Chem. Lett.* **2013**, *4*, 4074-4079.
(22) Torrent-Sucarrat, M.; Ruiz-Lopez, M. F.; Martins-Costa, M.; Francisco, J. S.; Anglada, J. M. *Chem. Eur. J.* **2011**, *17*, 5076-5085.
(23) Fukui, K. *Acc. Chem.. Res.* **1981**, *14*, 363-368.
(24) Tomasi, J.; Mennucci, B.; Cammi, R. *Chem. Rev.* **2005**, *105*, 2999-3093.
(25) Derbel, N.; Clarot, I.; Mourer, M.; Regnouf-de-Vains, J. B.; Ruiz-Lopez, M. F. *J. Phys. Chem. A* **2012**, *116*, 9404-9411.
(26) Collier, S. S.; Morikawa, A.; Slater, D. H.; Calvert, J. G.; Reinhardt, G.; Damon, E. *J. Am. Chem. Soc.* **1970**, *92*, 217-218.
(27) Kroll, J. A.; Frandsen, B. N.; Kjaergaard, H. G.; Vaida, V. *J. Phys. Chem. A* **2018**, *122*, 4465-4469.
(28) Anglada, J. M.; Martins-Costa, M. T. C.; Francisco, J. S.; Ruiz-López, M. F. *Phys. Chem. Chem. Phys.* **2019**, *21*, 9779-9784.
(29) Elliot, A. J.; McCracken, D. R.; Buxton, G. V.; Wood, N. D. *J. Chem. Soc. Faraday Trans.* **1990**, *86*, 1539-1547.
(30) B. J. Finlayson-Pitts; Pitts Jr, J. N. *Atmospheric Chemistry: Fundamental and Experimental Techniques*; Wiley: New York, 1986.